J. Fluid Mech. (1999), *vol.* 392, *pp.* 155–181. Printed in the United Kingdom

Flow field and noise characteristics of a supersonic impinging jet

By A. KROTHAPALLI, E. RAJKUPERAN, F. ALVI AND L. LOURENCO

Department of Mechanical Engineering, Florida A & M University and
Florida State University, 2525 Pottsdamer Street, Tallahassee, FL 32310, USA
e-mail: kroth@fmrl.fsu.edu

(Received 24 June 1998 and in revised form 13 March 1999)

This paper describes the results of a study examining the flow and acoustic characteristics of an axisymmetric supersonic jet issuing from a sonic and a Mach 1.5 converging–diverging (C–D) nozzle and impinging on a ground plane. Emphasis is placed on the Mach 1.5 nozzle with the sonic nozzle used mainly for comparison. A large-diameter circular plate was attached at the nozzle exit to measure the forces generated on the plate owing to jet impingement. The experimental results described in this paper include lift loss, particle image velocimetry (PIV) and acoustic measurements. Suckdown forces as high as 60% of the primary jet thrust were measured when the ground plane was very close to the jet exit. The PIV measurements were used to explain the increase in suckdown forces due to high entrainment velocities. The self-sustained oscillatory frequencies of the impinging jet were predicted using a feedback loop that uses the measured convection velocities of the large-scale coherent vortical structures in the jet shear layer. Nearfield acoustic measurements indicate that the presence of the ground plane increases the overall sound pressure levels (OASPL) by approximately 8 dB relative to a corresponding free jet. For moderately underexpanded jets, the influence of the shock cells on the important flow features was found to be negligible except for close proximity of the ground plane.

1. Introduction

While hovering in close proximity to the ground, short take-off and vertical landing (STOVL) aircraft experience a suckdown force, commonly known as 'lift loss'. This lift loss is due to the entrainment flow associated with the lifting jets which induce low surface pressures on the airframe resulting in a force opposite to lift. The lift loss in hover increases in magnitude as the aircraft approaches the ground. When the aircraft is in vertical landing mode and is near touch down, in addition to lift loss, the impingement of the high-speed lifting jets on the ground plane lead to significant ground erosion (Margason *et al.* 1997). Increased overall sound pressure levels (OASPL) associated with the supersonic jets are also of concern with respect to sonic fatigue of structural elements in the vicinity of the nozzle exhaust. These problems become more severe when the jets operate at supersonic speeds, which is the case in the future generation STOVL aircraft (e.g. the Joint Strike Fighter). Very limited data are currently available in the literature to characterize accurately the supersonic jet induced effects in hover. Using the simple configuration shown in figure 1, a series of experiments is conducted aimed at providing some understanding of the flow physics and identifying the main effects contributing to the hover lift loss.

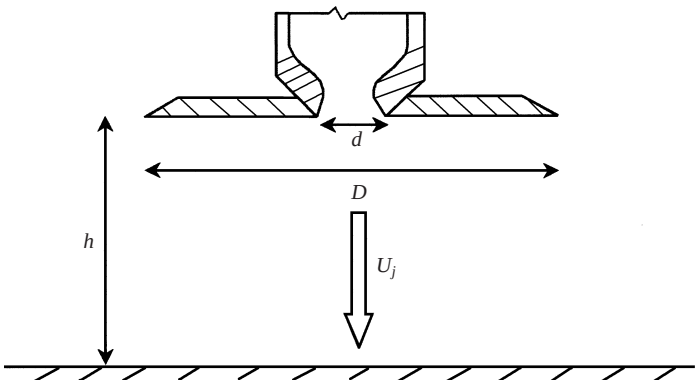

FIGURE 1. Schematic of the experimental set-up.

With the exception of the lift plate, the configuration chosen for this investigation closely resembles that used by a number of other investigators (Marsh 1961; Neuwerth 1974; Ho & Noisseir 1981; Powell 1988; Tam & Ahuja 1990; Henderson & Powell 1993; Messersmith 1995; Kuo & Dowling 1996) for the study of discrete sound generation of normally impinging jets. One of the key findings of these investigations is that the oscillation of the jet becomes a dominant feature of the flow when the ground plane is in close proximity to the jet exit. These oscillations are accompanied by high intensity sound ($\sim$160 dB, when the ground plane is at a distance of approximately 10 diameters) whose spectrum is dominated by discrete tones. In the past, the focus has been upon characterizing these tones and their generation mechanisms, especially in subsonic jets.

1.1. *The feedback mechanism*

The resonance-like behaviour of sound-producing oscillations is generally explained using a feedback loop that has its origins as far back as 1912. However, most of the current understanding of the feedback mechanism comes from the work of Powell (1953*a*, *b*). In his seminal paper (1953*a*), Powell not only discusses the physical mechanism governing feedback but also provides a simple feedback formula for predicting the frequencies of discrete tones so generated.

Although the formula proposed by Powell was mainly in the context of edge tones from high-speed jets, it applies equally well to impinging tones which, as pointed out by many investigators, including Powell himself (Neuwerth 1974; Ho & Noisseir 1981; Powell 1988; Tam & Ahuja 1990; Henderson & Powell 1993), are also generated by a feedback loop. Tam & Ahuja noted that the energy for the feedback loop is provided by the instability waves in the shear layers of the jet. These waves are generated by acoustic excitation in the region near the nozzle exit. The waves grow as they propagate downstream and manifest themselves as large-scale vortical structures that are commonly seen in flow-visualization pictures (cf. § 3). Upon impingement on the wall, these large structures generate coherent pressure fluctuations, which result in acoustic waves with significant intensity, sufficient to render them visible in shadowgraph pictures. The acoustic waves travel through the ambient medium and upon reaching the nozzle exit, excite the shear layer of the jet, leading to the generation of instability waves thus closing the feedback loop. Krothapalli (1985) used the feedback-loop mechanism to predict the frequencies generated by an impinging supersonic rectangular jet, thus verifying its validity. When the impinging plate size is

small (a few jet diameters), additional tones are observed (Powell 1988; Henderson & Powell 1993) that relate to flow features associated with the oscillations of the normal standoff shock (cf. § 3). Such standoff shocks are observed in experiments using underexpanded jets. When the jets are 'highly underexpanded' the oscillations of the Mach disk also appear to play a role in the feedback mechanism (Glaznev 1977).

The present study is concerned with the sound produced by axisymmetric supersonic jets exiting either from a converging–diverging (C–D) nozzle or a converging choked nozzle at moderate nozzle pressure ratios (NPR), where NPR is defined as the ratio of the stagnation pressure to the ambient pressure. In the present experiments NPR is less than 6. The plate representing the ground plane upon which the jet impinges is very large compared to the jet diameter (4000d, where d is the nozzle throat diameter). More details of the experimental hardware are discussed in § 2.

In the present context, it is believed that the phenomenon associated with discrete sound generation is governed by the simple acoustic feedback loop as discussed earlier. The impingement tone frequency f_N is determined from the following formula proposed by Powell (1953*a*):

$$\frac{N+p}{f_N} = \int_0^h \frac{\mathrm{d}h}{C_i} + \frac{h}{C_a} \quad (N = 1, 2, 3, \ldots). \tag{1}$$

Here h is the distance between the wall and the nozzle exit and C_i and C_a are the convection velocities of the downstream-travelling large structures and the speed of upstream-travelling acoustic waves, respectively. N is an arbitrary integer and p represents a phase lag due to the fact that the phases of the acoustic wave and of the convected disturbance are not always exactly equal at both the nozzle exit and the source of the sound.

In order to predict the impinging tone frequencies using the above formula, accurate values of the large-scale structure velocities are needed. Owing to the difficulty of measuring these velocities experimentally, especially in supersonic jets, most previous investigators assumed a constant value for C_i— usually in the range of 60% to 70% of the primary jet velocity. The results presented later will show that this is not always the case; rather, the propagation speeds of the large structures exhibit significant variation with plate height. For example, the measured convection velocity of identifiable vortical structures in the shear layer of the free jet was found to be about 0.6 U_j, where U_j is the fully expanded jet velocity, whereas, for an impinging jet, it was found to be about 0.5 U_j at $h/D = 4$. Karamcheti *et al.* (1969) also found such variation in the convection velocity in earlier low-speed edge tone experiments.

In this paper, we will verify the validity of the simple feedback formula using the present experimental data. The uniqueness of this comparison lies in the fact that the convection velocities of the downstream-travelling large-scale structures (C_i) used in the formula were obtained directly from velocity measurements using the PIV technique. Recent theoretical attempts by Tam & Ahuja (1990) and Kuo & Dowling (1996), using linear stability analysis, provided better models for the frequency determination. The amplitude prediction of the tones, which are of primary interest in practical applications, still remains elusive. However, using computational tools, progress is being made by How & Tam (1998) to predict the amplitude of screech tones.

1.2. *Broadband noise*

In addition to the discrete sound generated due to a feedback loop as described above, the broadband noise also becomes important as it contributes to an increase

in the OASPL for an impinging jet by approximately 10 dB, relative to a free jet. The full-scale noise investigations of Harrier aircraft by Soderman (1990) suggest that the strong jet oscillations discussed above may be an artifact of small-scale laboratory cold jets. However, when two jets are in close proximity, as is the case in the proposed Boeing Joint Strike Fighter (JSF) configuration, a strong flow-acoustic coupling occurs between the two jets resulting in violent oscillations. These oscillations may lead to sonic fatigue of the nearby structures.

When the jet approaches the ground, the OASPL levels increase significantly as will be shown in § 3. In addition to the commonly known sources of sound from free supersonic jets, such as mixing noise and shock associated noise, the increased levels may also be attributed to the acoustic reflection from the ground, and the generation of additional noise sources in the jet impingement and wall-jet region of the flow field. The reflection of jet noise by the ground was modelled by Sutherland & Brown (1972) using an array of image sources placed symmetrically with respect to the ground plane where both sources (due to the jet) and their images radiate into unbounded space. Acoustic amplifications of up to 14 dB were predicted using this simple model. However, experimental observations by Soderman (1990) indicate much lower amplification levels.

To the authors' knowledge, measurements regarding the aeroacoustic behaviour of full-scale supersonic impinging jets (heated or cold) are not currently available in open literature. However, investigations of small-scale supersonic heated free jets show the presence of screech tones governed by a feedback mechanism similar to the impingement tones of the present study (see Krothapalli *et al.* 1997 for more details and references). Typically, in high-temperature supersonic jets, the broadband mixing noise levels are high enough to disguise the discrete tones (Krothapalli *et al.* 1997) and, as a result, their contribution to the OASPL is minimal. In light of the presence of screech tones in hot model jets we believe that impingement tones may persist in full-scale STOVL aircraft, i.e. in full-scale, hot, supersonic impinging jets.

There is clearly a lack of high-quality data information in the literature necessary to accurately model the noise generated by a supersonic jet impinging on the ground. In particular, the prediction of OASPL still remains elusive. The present study is an attempt to provide quality baseline data that can provide some insight into the flow physics as well as guidance for modelling efforts and their validation.

1.3. *Hover lift loss*

The loss of lift in STOVL aircraft while in hover mode has been extensively studied for subsonic aircraft where the impinging jets are also subsonic or subcritical. A good discussion of this issue, especially for subsonic jets, may be found in Margason *et al.* (1997). Briefly, the entrainment of the ambient fluid by the primary lifting jet(s) induces low pressures on the lower surface of the airframe, which in the present configuration is represented by a circular lift plate. Additional entrainment by the radial wall jet formed because of the impingement of the lifting jet can further reduce the surface pressures on the lift plate. It is expected that the entrainment due to the wall jet will become more significant when the ground plane is in close proximity to the nozzle exit and the ambient region from which the fluid is entrained becomes increasingly confined. As a result of the low surface pressures, a force in a direction opposite to the jet thrust is created, leading to a lift loss. The magnitude of this suckdown force and lift loss increases as the ground plate approaches the nozzle exit. As a consequence of the above mechanism responsible for lift loss, it is expected that increasing the jet entrainment would result in a higher lift loss. Based on extensive

data, this fact has been established for subsonic jets which show that jets which decay rapidly in terms of the centreline velocity (presumably due to higher entrainment rates), induce increased flow along the lower surface of the lift plate, resulting in reduced surface pressures and an increased lift loss (Margason *et al.* 1997).

In contrast to subsonic flows, very few data are at present available for supersonic impinging jets in STOVL configurations. In a recent study, researchers observed a nonmonotonic lift loss as a function of jet NPR for a supersonic impinging jet (Levin & Wardwell 1997). From the flow-visualization data, they speculated that this nonlinear lift loss behaviour may be related to the jet shock cell structure; however, a more rigorous explanation remains elusive. One of the objectives of this study is to investigate the lift loss phenomenon for supersonic impinging jets and to examine the physical mechanism responsible for this behaviour. Among other parameters, the role of shock cells on lift loss will also be examined. It is also well-known that jets with self-excited oscillations at discrete frequencies decay more rapidly than their counterparts without the oscillations. Hence, it is of interest to establish whether there is a correlation between the oscillatory behaviour of the jet column and the hover lift loss. It should be noted that other ground effects associated with single and multiple impinging jets, such as: ground erosion; fountain flow; and pitching moment due to the roll-up of a wall jet into a horseshoe-shaped ground vortex in transition to forward flight, can also significantly affect aircraft performance (Kuhn 1997). However, these issues will not be addressed in the present paper.

Keeping the above observations in mind, a basic research program has been initiated to investigate the aeroacoustics of supersonic single and multiple impinging jets. In this paper, the results of an investigation of the near sound field and the lift loss characteristics generated by an axisymmetric supersonic jet issuing from a convergent and a C–D nozzle are presented.

2. Experimental apparatus and procedures

The details of the hover test facility used for the experiments discussed in this paper are given by Wardwell *et al.* (1993). The facility was designed to obtain the jet-induced forces on STOVL model aircraft hovering in and out of ground effect. In order to simulate different heights above the ground, the ground plane is mounted on a hydraulic lift and can be moved relative to the model (figure 2). For the experiments described here, the ground plane was 2.44 m $\times$ 2.44 m and was centred underneath the model. To obtain measurements in the ground plane for ground erosion studies, a secondary instrumented 2.54 cm thick, 1 m $\times$ 1 m Plexiglas plate was mounted on the larger ground plane.

Two different nozzles were used in this study. A converging axisymmetric nozzle with an exit diameter of 2.54 cm was used to simulate an underexpanded choked jet. A shock-free nearly ideally expanded jet was obtained using a C–D axisymmetric nozzle with a throat diameter of 2.54 cm designed for an exit Mach number of 1.5. The exit diameter of the C–D nozzle was 2.75 cm. The divergent portion of the nozzle was a straight conic section with a 3° divergence angle to mimic the realistic nozzle geometry used in practice. Several nozzles were made with different diverging angles to study its influence on the lift loss. However, the data in this paper is restricted to the 3° nozzle. The nozzle upstream of the throat was designed using a third-order polynomial with a contraction ratio of approximately 5.

A high-pressure blow-down compressed air facility was used to supply air to the nozzles. A high-displacement reciprocating air compressor drives the facility, which

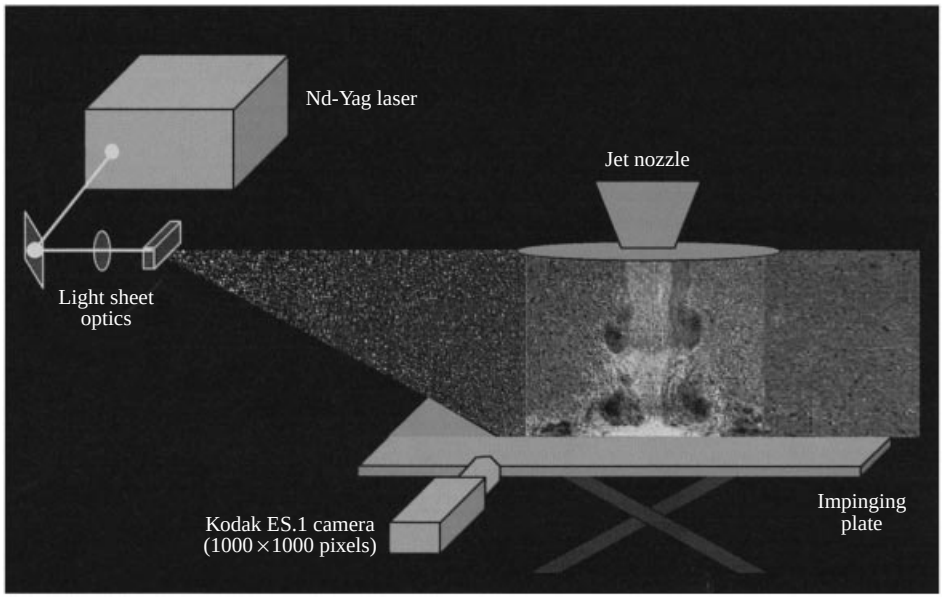

FIGURE 2. Schematic of the PIV set-up.

is capable of supplying air at a maximum storage pressure of 160 bars. Large storage tanks provide a total capacity of 10 m^3 and are capable of driving the Mach 1.5 jet continuously up to 40 min.

The nozzle was flush mounted with a circular lift plate of diameter D, as shown in figure 1. The lift plate diameter is 25.4 cm (approximately ten times the nozzle exit diameter) and is instrumented with 17 surface pressure taps along a radial line. The pressure taps are used to obtain detailed surface pressure distribution on the lift plate. The taps are more closely spaced near the nozzle exit where the mean pressure variations are expected to be more significant. The pressures were measured with a Validyne strain-gauge transducer mounted in a Scanivalve unit. At each port, several seconds of digitized data was recorded to obtain the mean surface pressure. The jet-induced mean surface pressure distributions were subsequently used to calculate the lift force on the plate.

A shadowgraph system with a field of view of 30 cm was used to visualize the flow field. It employed a conventional single-pass arrangement with a stroboscopic flash unit having a flash duration adjustable from 1.3 to 7 μs at five discrete settings. The frequency of the pulsed light source can be varied up to a maximum of 1 kHz.

In the particle image velocimetry experiments, the jet was seeded with small ($\sim$ 1 μm) oil droplets generated using a modified Laskin nozzle. The ambient air was seeded with smoke particles ($\sim$ 5 μm in diameter) produced by a Rosco fog generator. A schematic of the experimental arrangement of the PIV system is shown in figure 2. Because of the unique nature of the PIV measurements used in this study, a brief description of this technique is provided in the following section.

Near-field acoustic measurements were obtained using a 0.635 cm diameter B & K microphone oriented 90° to the jet axis and placed approximately 25 cm away from the nozzle exit. The conditioned signals from the microphone and the surface pressures on the lift plate were acquired using a National Instruments data acquisition system with associated 'LabView' software. For acoustic measurements, the nearby exposed metal surfaces were covered with 10 cm thick acoustic foam to minimize sound reflections.

The main controlling parameters in the experiment were as follows: nozzle pressure ratio (NPR), which was varied from 1.5 to 5.5; the ground plate height h with respect to the nozzle exit, varied from $2.5d$ to $60d$ (d, diameter of the nozzle throat = 2.54 cm). The jet stagnation temperature was nominally maintained at 20°C. A top-hat velocity profile with laminar boundary layers was maintained at the nozzle exit. The nominal exit Reynolds number was 7×10^5.

2.1. *Particle image velocimetry*

The main feature of the particle image velocimeter used in this experiment is its ability to record two images in quick succession, from which the velocity field is derived using a cross-correlation algorithm. This is possible by integrating the PIV system's two main hardware components: the Kodak ES1.0 digital video camera and the dual Spectra Physics Nd-Yag laser illumination system, with a repetition rate of 15 Hz. At the heart of the camera is the CCD interline transfer sensor, KAI-1001 with a resolution of 1008(H) × 1018(V) pixels. Each square pixel measures 9 μm on the side with 60% fill ratio with a microlens, and a centre to centre spacing of 9 μm. The camera is also equipped with a fast electronic shutter and outputs eight-bit digital images, via a progressive scan readout system, at a rate of 30 frames per second.

The arrangement described above makes it possible to acquire up to 15 image pairs per second. The fact that the image pairs are recorded in separate frames and that the image pair separation can be reduced to a few microseconds makes this instrument appropriate for high-speed flows. In the present experiments, a 2 μs pulse separation was used. The image is acquired from the camera using an Imaging Technologies ICPCI board, which resides on a single slot of the PCI bus of a personal computer. The computer CPU is an Intel 300 MHz Pentium with 256 Mbytes of RAM, running under the Windows NT operating system.

An image-matching approach is used for the digital processing of the image pairs to produce the displacement field. One of the shortcomings of the conventional processing scheme is the spatial resolution. This limitation is due to the averaging caused by the typical correlation window size, of the order of 16^2–32^2 pixels. Since the measurement represents an average over the correlation window, it can be weighted towards the areas of the window with higher seeding density and/or reduced velocity. This weakness especially limits the use of this technique in flows with large velocity and/or seeding density gradients, e.g. reacting flows.

To achieve velocity data with high spatial resolution a novel processing algorithm was developed (Lourenco & Krothapalli 1998). With the new processing approach, the particle images themselves comprise the interrogation region, which have sizes ranging from 3 to 4 pixel square. Such a high-resolution scheme not only allows for accurate measurements of the gradient fields but also permit measurements in very close proximity of solid surfaces.

The displacement between image pairs was found in the usual manner by means of cross-correlation, and a velocity (displacement) vector is assigned at the mid-distance between image pairs. Therefore, each particle pair contributes to a second-order approximation of the velocity. However, in contrast to the traditional approach which uses structured grids, these velocities are evaluated in an unstructured grid. The flow field at any point is described by an analytical function using a least-squares-fitting algorithm. The function that is used is a second-order polynomial:

$$\boldsymbol{u} = \boldsymbol{a}x^2 + \boldsymbol{b}x + c\boldsymbol{y}^2 + \boldsymbol{d}y + \boldsymbol{e}xy + \boldsymbol{f}. \tag{2}$$

The marked advantage of this approach is that the field is described at any point with

second-order accuracy, including the derivatives that are found by differentiating the previous equation, given as

$$\left.\begin{aligned} \frac{\partial}{\partial x}\boldsymbol{u} &= 2\boldsymbol{a}x + \boldsymbol{b} + \boldsymbol{e}y, \\ \frac{\partial}{\partial y}\boldsymbol{u} &= 2\boldsymbol{c}y + \boldsymbol{d} + \boldsymbol{e}x. \end{aligned}\right\} \tag{3}$$

Although an unstructured grid is used for calculating the velocity, for ease of visualization, the velocity field is usually presented at regular intervals. This new scheme is very efficient and incorporates a vector validation procedure, making it independent of operator intervention. The time it takes to compute a vector field depends on the computer hardware and it ranges from 1400 mesh points s^{-1} on a 200 MHz dual Pro Pentium PC up to several thousand on a 500 MHz Alpha based PC.

Despite the use of the novel processing scheme described above, some particle lag always occurs, especially in regions with very high velocity gradients, such as in the vicinity of shock waves. A careful study examining the behaviour of particles in supersonic flows with shocks was conducted by Ross, Lourenco & Krothapalli (1994) using a similar PIV system. As expected, the particle relaxation time was found to be a strong function of the particle diameter and shock strength. Consequently, it is expected that the location of strong shocks will be somewhat 'smeared' owing to particle lag, a fact noted in a subsequent discussion of velocity profiles obtained from PIV measurements (cf. § 3.2, figure 13*b*). Similar particle lag will also occur in other regions with high velocity gradients such as the wall jet although this effect will be of a lesser degree than that across a shock. A more detailed investigation, which is outside the scope of this study, is required to assess the particle behaviour accurately in regions with large velocity gradients and highly rotational flows such as the large-scale vortical structures and the near-wall region of the wall. However, in the absence of shock cells the mean velocity field data obtained using PIV shows that the velocity of the particles is in very good agreement ($\pm 1\%$) with the exit velocity calculated using isentropic relations. Furthermore, instantaneous velocity field data, such as that shown in figure 8, clearly reveals that the PIV technique is capable of capturing the presence of large-scale structures in the primary jet and the wall jet. Despite the uncertainty introduced because of particle lag, it is expected that the effects of shocks and large-scale vortical structures do not significantly alter the conclusions reached in this investigation and are of ancillary importance in this study.

3. Results and discussion

3.1. *Flow visualization*

A conventional shadowgraph technique was used to visualize the jet flow. The images were captured using an SVHS video camera. Selected images displaying important flow and acoustic features are shown in figures 3–5 and will be discussed in this section.

It is well known that the axisymmetric free-jet instability manifests itself in symmetric as well as helical and/or flapping modes depending upon the exit Mach number, NPR (i.e. over/under-expansion condition), and the exit boundary-layer characteristics. The mode type also depends upon the height of the ground plane with respect to the nozzle exit. The flow-visualization images of an ideally expanded free jet at

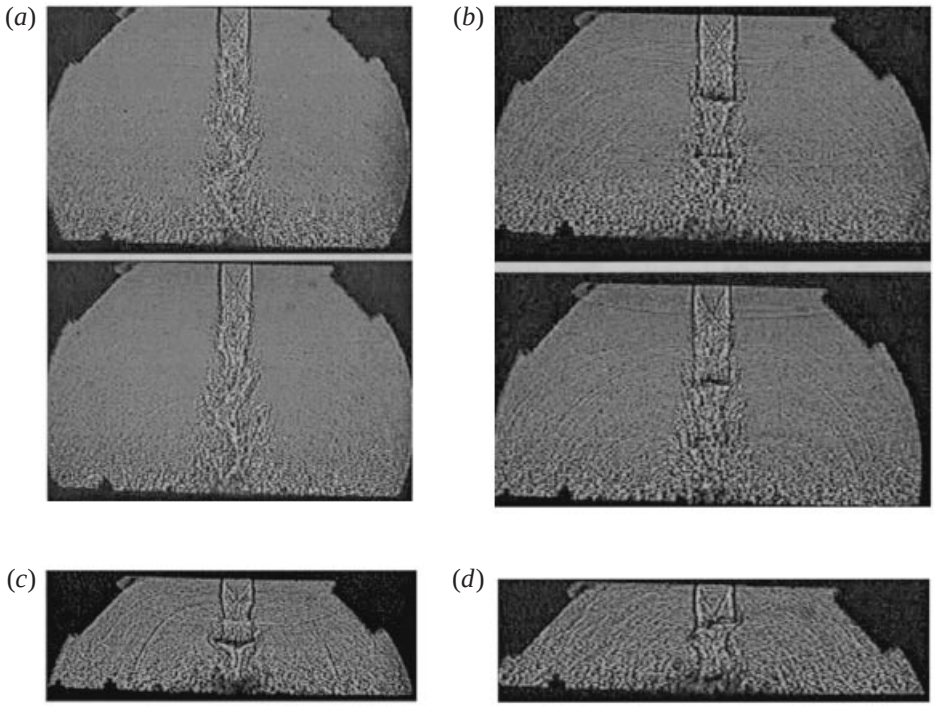

FIGURE 3. Instantaneous shadowgraphs depicting helical and symmetric modes of an ideally expanded supersonic impinging jet at $M = 1.5$. (*a*) $h/d \sim 8$; (*b*) $h/d \sim 6$; (*c*) $h/d \sim 4$; (*d*) $h/d \sim 3$.

$M = 1.5$ (not shown here) suggest that this jet is dominated by the helical mode instability. When the impinging plate is present, the helical mode continues to dominate up to $h/d \sim 8$, as shown in figure 3(*a*). Note that, in these and subsequent images, the lift plate and the ground plane appear as dark horizontal lines on the top and bottom of the pictures, respectively. The two pictures included in figure 3(*a*) represent the jet at two different phases of the resonance condition. An examination of the continuous video record suggests that the acoustic modes allowed at these conditions are also asymmetric in nature. When the ground plane is moved closer to the jet exit to $h/d \sim 6$, the axisymmetric mode begins to dominate, as shown in figure 3(*b*). The axisymmetric nature of the flow is also evident by the presence of the symmetric large-scale turbulent structures in the jet. The axisymmetric instability and acoustic modes persist until $h/d \sim 4$ (figure 3*c*). A further decrease in ground plate distance results in the re-emergence of the helical mode, as shown in figure 3(*d*). Also evident from figures 3(*b*) and 3(*c*) are the incident and reflected acoustic waves in the jet near field. The incident waves are concave upwards and travel upstream (relative to the primary jet flow) while the waves reflected by the lift plate are of opposite curvature and travel downstream in the ambient medium. Owing to the straight divergent section and finite nozzle lip thickness, a weak shock cell structure is present in the jet. The presence of only a weak shock cell structure precludes the generation of screech, a fact verified by the acoustic measurements.

A better illustration of the incident and reflected acoustic waves is seen in figure 4(*a*) where the ground plane is at $h/d \sim 4$. Also seen clearly in the image are the downstream-propagating axisymmetric structures in the jet column. The source of the upstream-propagating acoustic wave system be identified in the picture by locating

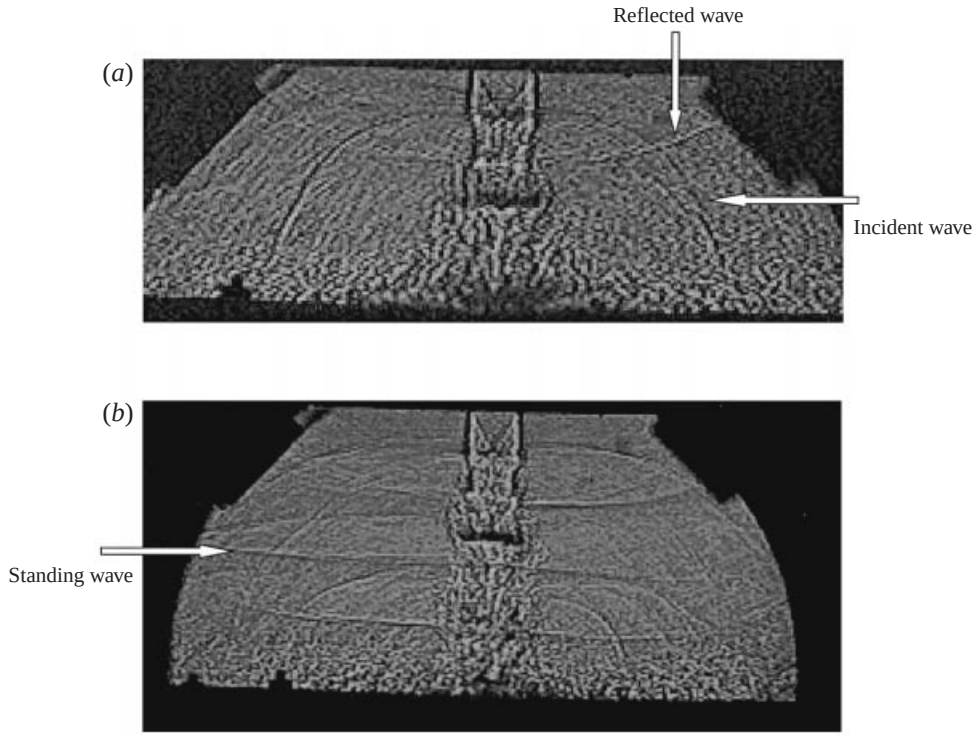

FIGURE 4. Instantaneous shadowgraphs depicting helical and symmetric modes of an ideally expanded supersonic impinging jet at $M = 1.5$. (*a*) $h/d \sim 4$; (*d*) $h/d \sim 5.5$.

the centre of the arcs. This source location is found to be in the stagnation region on the ground plane. Additionally, under certain conditions, a standing wave pattern is also produced between the lift plate and the ground plane, as shown in figure 4(*b*). The wavelength between the successive upstream-propagating acoustic waves roughly corresponds to a frequency calculated from the feedback loop (cf. § 3.4). The standing wave pattern represented by the horizontal lines corresponds to another resonance frequency that depends upon the distance between the lift plate and the ground plane (Krothapalli & Hsia 1996).

When the jet is moderately underexpanded, at NPR = 5, a series of shock cells appears as shown in figure 5(*a*). To accentuate the features of the shock cell structure, time-averaged (average of 17 instantaneous images) shadowgraph images are presented here. In the presence of a shock cell structure, when the ground plane is close to the jet exit, the most notable feature is the generation of a stand-off or plate shock which in some cases is accompanied by a local stagnation bubble in the impingement region. The stand-off shock can be seen in figures 5(*b*)–5(*d*) while the bubble can be observed in figure 5(*c*) and is indicated on the image for clarity. Although the stand-off shock was not observed for $h/d > 8$, it was not always present for all conditions corresponding to $h/d < 8$; in fact its size, shape and presence is a strong function of NPR and h/d. The appearance and disappearance of the shock and the associated separation or stagnation bubble may play an important role in determining the local aerodynamic and acoustic field, thereby affecting the lift loss and acoustic loading (cf. § 3.3 and 3.4). The oscillations of the underexpanded jet were quite similar to those observed in figure 4 and both axisymmetric and helical modes

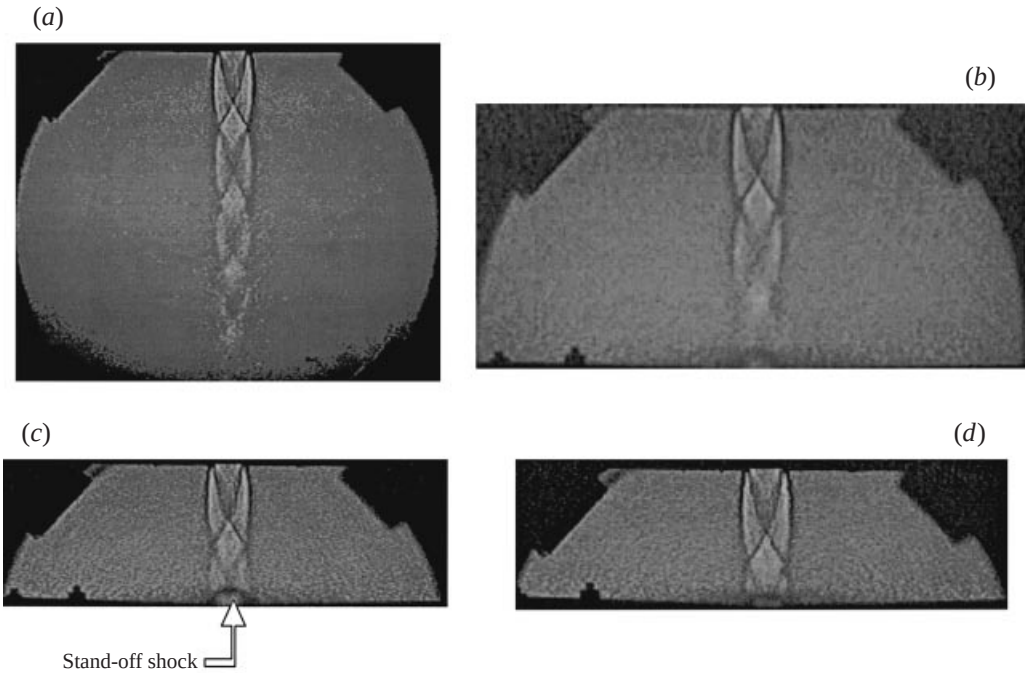

FIGURE 5. Mean shadowgraphs of an underexpanded supersonic jet at NPR = 5.0 for $M = 1.5$ C–D nozzle. (*a*) $h/d \sim 60$; (*b*) $h/d \sim 6$; (*c*) $h/d \sim 4$; (*d*) $h/d \sim 3.4$.

of oscillation were observed. Henderson & Powell (1993) considered the stand-off shock distance from the ground plane and different disturbance convection velocities upstream and downstream of the stand-off shock region to calculate the self-excited oscillation frequency (cf. §§ 3.4). The flow associated with the stand-off shock has been the focus of several investigations (Lamont & Hunt 1980). The detailed discussion of this aspect is outside the scope of the present paper, since it is more pertinent to the ground erosion problem.

3.2. *PIV flow-field measurements*

A detailed investigation of the jet characteristics was carried out using the PIV technique. All the measurements are confined to the central plane of the jet. Typical double exposure images of the free jet and the impinging jet are shown in figure 6. The main jet is seeded with the oil droplets while the ambient medium is seeded with smoke particles. The flow field produced by the jet impingement consists of three flow regimes: the free jet upstream of the ground plane, the impingement region and the wall jet. Donaldson & Snedeker (1971) provide a very good discussion of the basic flow characteristics of these regions, especially, the mean flow. The focus of the PIV measurements is the unsteady characteristics of the flow field and their effect on lift loss. Hence, little attention is paid here to the radial wall-jet flow field on the ground plane. However, a companion investigation is currently underway to investigate the impingement and the accompanying wall-jet regions (Alvi & Iyer 1999).

For the case of a free, nearly ideally expanded jet, shown in figure 6(*a*), there are no discernible large-scale organized structures such as those found in figure 6(*b*) which corresponds to an impinging jet at $h/d = 4$. The large structures appear to be nearly symmetrical, corresponding to the axisymmetric nature of this flow, also observed

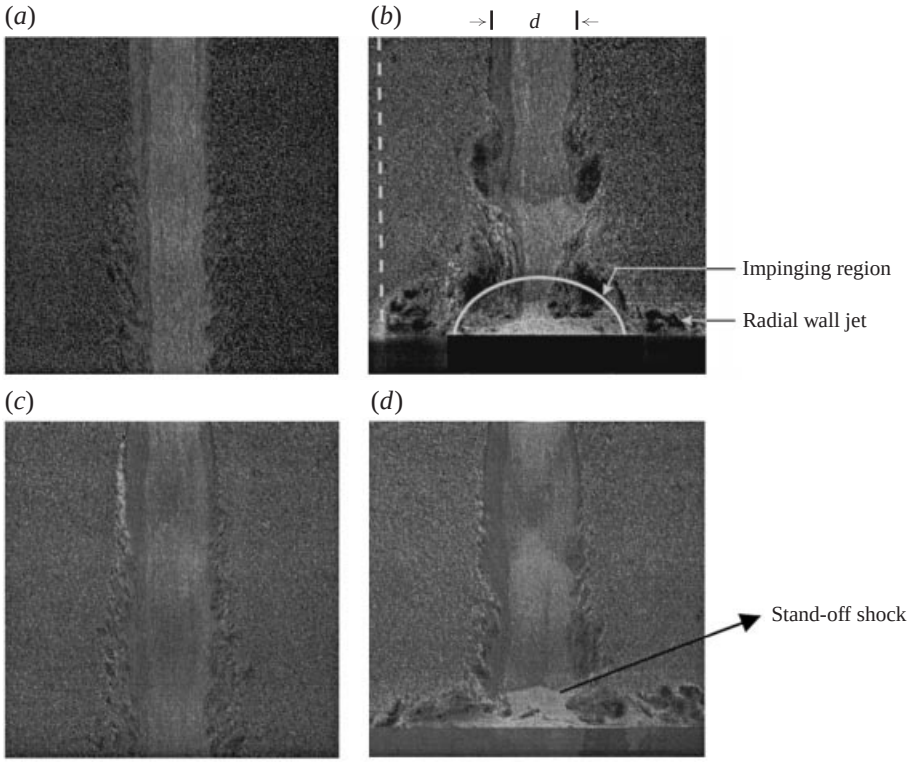

FIGURE 6. Instantaneous PIV images for $M = 1.5$ C–D nozzle. (*a*) Ideally expanded free jet, NPR = 3.7; (*b*) ideally expanded impinging jet, NPR = 3.7, $h/d = 4$, vertical dotted line is measurement location for entrainment velocity, q; (*c*) underexpanded free jet, NPR = 5.0; (*d*) underexpanded impinging jet, NPR = 5.0, $h/d = 4$.

earlier in figure 3. Upon impingement on the ground plane, the structures move laterally in the radial wall jet without losing much of their coherence. In the case of an underexpanded jet at NPR = 5 (figure 6*c*), the vortical structures appear to be smaller and much less organized relative to those shown in figure 6(*b*). The stand-off shock, a prominent feature of this flow, is indicated by an arrow in figure 6(*d*).

The instantaneous velocity field was obtained by the method described in § 2.1, with interrogation regions of 8×8 pixels corresponding to a physical dimension of 0.8×0.8 mm. The data was obtained using a $120 \times 80(x, r)$ Cartesian grid. Typical instantaneous velocity fields corresponding to the images in figure 6 are shown in figure 7. The magnitude of the out-of-plane component of the vorticity shown in colour contours is superimposed on the velocity field. In this fashion, the identity of large-scale vortical structures in the shear layer of the jet can be accentuated. Forty such instantaneous velocity fields were obtained for each of the condition tested.

One of the key parameters in the frequency prediction formula given in § 1.1 is the convection velocity of the large-scale structures, C_i. In the absence of any direct measurements of the convection velocity, many of the previous investigators estimated its value to be between 0.6 and 0.7 U_j (U_j: mean jet exit velocity). From the velocity field data, it is possible to identify the regions of concentrated vorticity. For example, a typical region of high vorticity corresponding to a coherent vortical structure is shown in figure 8. Once a structure is identified, its convection velocity can be obtained easily

from the velocity data. Free-jet convection velocities of 0.6 U_j were measured in this fashion. However, in the case of an impinging jet, the convection velocity varies as a function of the plate height and the NPR. Figure 9 shows the convection velocities measured from individual PIV images, each represented by a single data point on the plot. Obviously, the location of the large-scale vortical structures (given on the x-axis) varies from one PIV image to another. The solid line in the plot represents the average value of the convection velocity, which in this case is equal to 0.52 U_j. Because of the non-uniform variation of the centreline velocity owing to the presence of the shock cell structure, U_j is substituted here by a mean velocity, U_{clm}, obtained from averaging the centreline velocity of the free jet within the first five diameters.

As the plot in figure 9 shows, measurement of the convection velocities, C_i of large-scale structures were obtained only for $x \leqslant 75 \sim 80$ mm. This is typical for all the cases presented in this paper, where the convection velocity measurements could not be obtained in regions close to the wall. This is due to the presence of the impingement zone and the wall jet in the near-wall region which makes it very difficult, if not impossible, to identify large-scale structures and obtain reliable data for C_i. We suspect that the lack of this data may somewhat bias the average convection velocities towards higher values since one would expect the structures to slow down as they approach the ground plane. However, since the region where this occurs is relatively small, we expect the bias to be small and the convective velocities presented here to be fairly accurate. The variation of the average convection velocity with the plate height is shown in figure 10 for three different NPR. For example, for an ideally expanded jet (NPR = 3.7), the convection velocity increases linearly with h/d from 0.52 U_j at $h/d = 4$ towards the free-jet value. Figure 10 also shows that for a fixed h/d, the presence of shock cells increases the convection velocities of the vortical structures. From the flow visualization pictures (see figure 6) and PIV data, it appears that these vortical structures are much smaller in the presence of shock cells and are located mostly towards the high-speed side of the shear layer. The convective Mach number of the large structures, M_c, ($M_c = (U_{clm} - C_i)/a_j$; a_j is speed of sound in the jet) at NPR = 5 was found to vary from 0.73 at $h/d = 10$ to 0.66 at $h/d = 4$. These values are consistent with the measurements of Powell (1988) who derived them from the flow-visualization pictures.

The magnitude of the surface pressures on the lift plate is closely linked to the jet entrainment velocities in the near hydrodynamic field, especially when the jet is confined by two solid boundaries (lift plate and the ground plane). These velocities can be obtained easily from the PIV data. Typical instantaneous velocity variation with downstream distance at a radial location of $1.5d$ is shown in figure 11. Included in the figure are the data for a free jet and the impinging jet at two different pressure ratios. The magnitude of the near-field instantaneous entrainment velocity, $q(q = (u^2+v^2)^{1/2})$ for a free jet is about 8 m s^{-1}, while for the impinging jet, it can be as high as 50 m s^{-1}, as indicated by the peaks in the velocity plot. Such large velocities in the near hydrodynamic field correspond to the presence of large vortical structures which can be clearly seen in figure 7. These high entrainment velocities will result in suction pressures on the bottom surface of the lift plate resulting in a downward force (lift loss), details of which are discussed in the next section. The entrainment field is quite unsteady as seen from three different instantaneous velocity profiles at the same radial location, shown in figure 12. The large velocities seen in the region $x > 75$ mm correspond to the radial wall jet. The thickness of the radial wall jet changes with time as suggested by the location of the peak velocity magnitude close to the ground plane $x > 75$ mm (figure 12). From the examination of a number of instantaneous

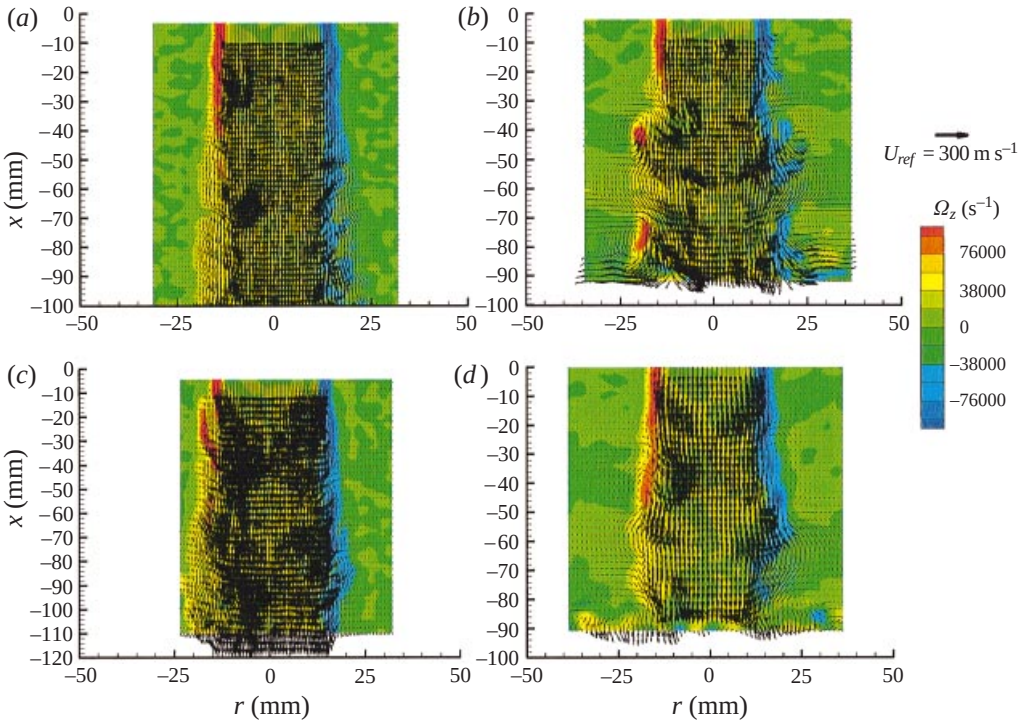

FIGURE 7. Instantaneous velocity fields corresponding to images shown in figure 6.

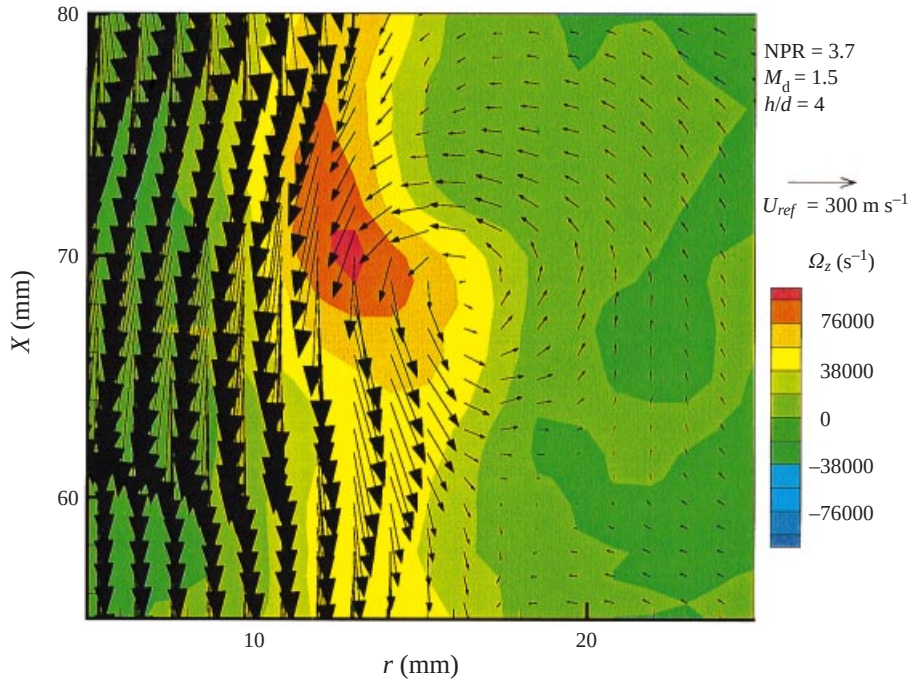

FIGURE 8. Details of the large-scale vortical structure. Underexpanded impinging jet, $M = 1.5$ C–D nozzle, NPR = 3.7, $h/d = 4$.

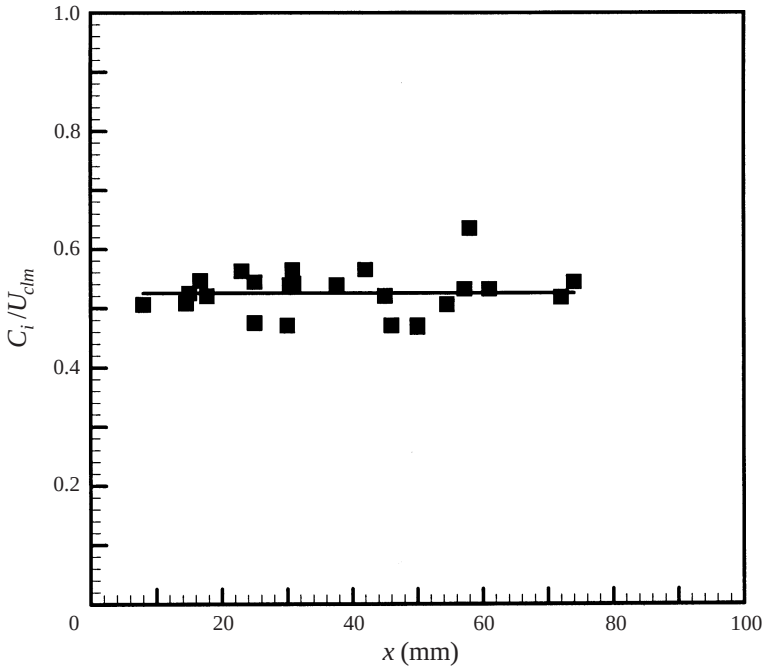

FIGURE 9. Instantaneous convection velocities of large-scale vortical structures obtained from PIV data. Ideally expanded impinging jet, NPR = 3.7, $h/d = 4$.

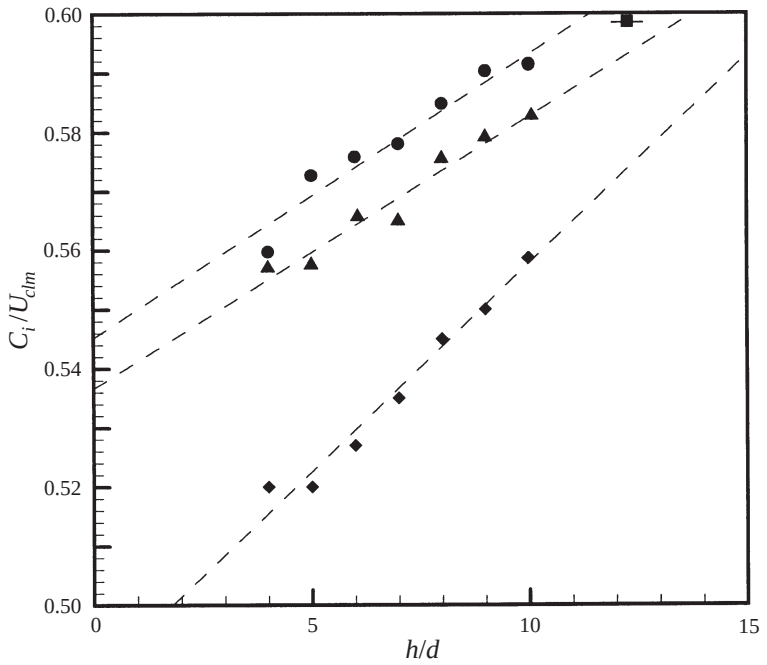

FIGURE 10. Variation of the normalized convection velocity of the large vortical structures with ground plane distance. ●, NPR=5.0; ◆, 3.7; ▲, 2.5; ■, Free jet $h/d = 60$.

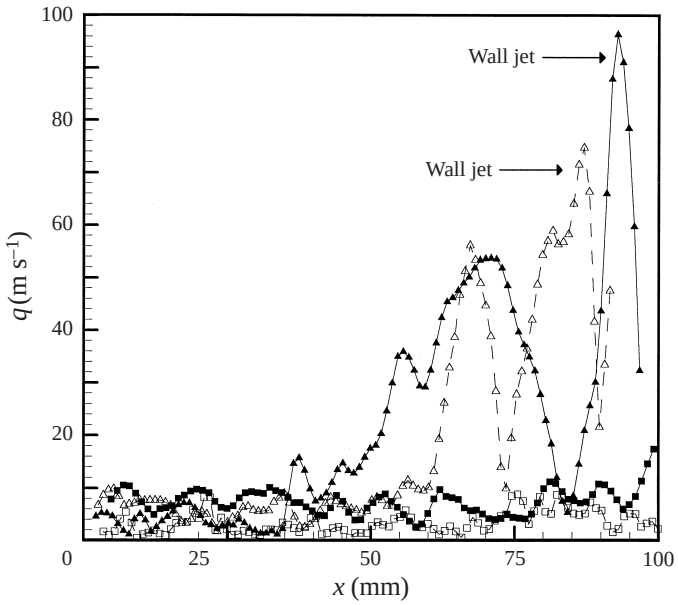

FIGURE 11. Instantaneous entrainment velocity for free and impinging jets at $r/d = 1.5$ (see figure 6). NPR=5.0: ■, freejet; ▲, $h/d = 4$; NPR=3.7: □, free jet; △, $h/d = 4$.

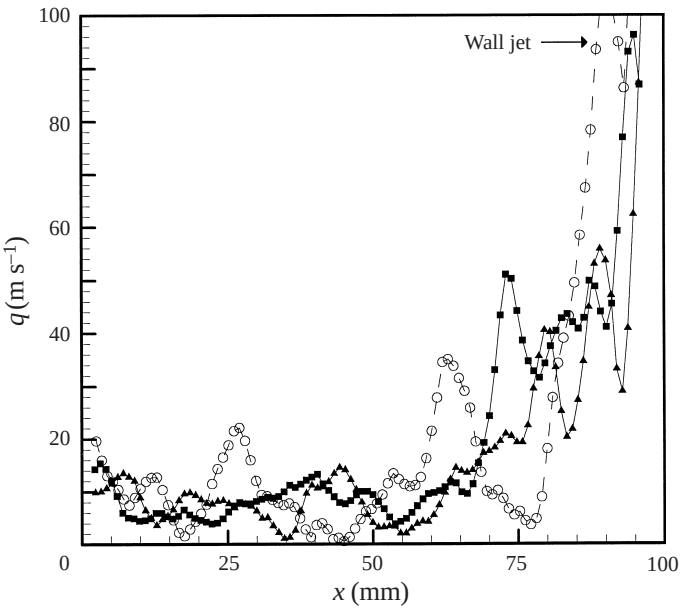

FIGURE 12. Instantaneous entrainment velocities at three different instances at $r/d = 1.5$. Underexpanded impinging jet, NPR = 5.0, $h/d = 4$.

velocity fields, it is observed that the wall jet is primarily characterized by the large vortical structures that orginate in the jet shear layer.

The mean velocity field was obtained by averaging 40 instantaneous velocity fields. The number of samples used here is not sufficient to obtain a true mean velocity field. However, the trends provided by the averaged data are adequate to observe the

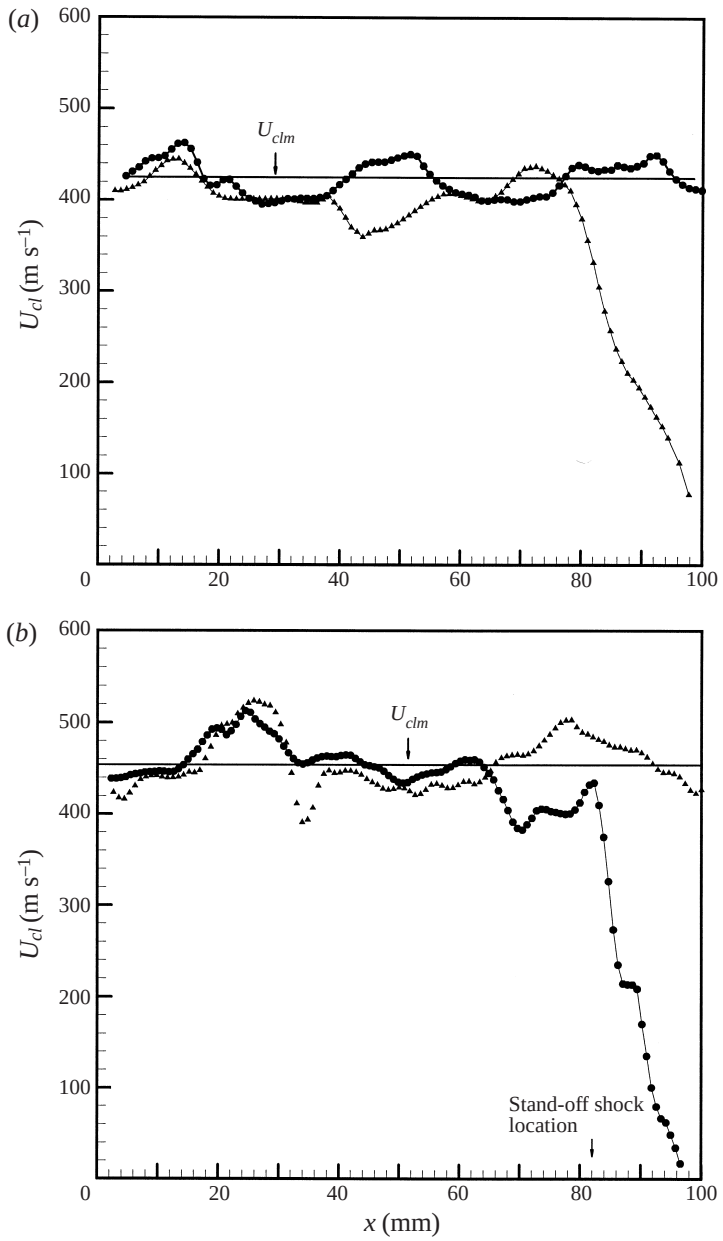

FIGURE 13. Mean centreline velocity variation for free and impinging jets. (*a*) NPR = 3.7; ▲, $h/d = 4$; ●, free jet; (*b*) NPR=5.0; ▲, free jet; ●, $h/d = 4$.

significant changes due to the impingement process. Figure 13 shows the centreline velocity variation with downstream distance for free and impinging jets. For the impinging jet, the ground plane was located at $x = 101.6$ mm ($x/d = 4$). The variation in the averaged centreline velocity in the free jet is primarily due to the shock cell structure. The spatial mean centreline velocity U_{clm}, calculated using the data from $x/d = 0.2$ to $x/d = 5$ for a free jet, is depicted by the solid line. For an impinging jet at NPR = 3.7, the mean centreline velocity remains nominally constant up to $x/d \sim 3$.

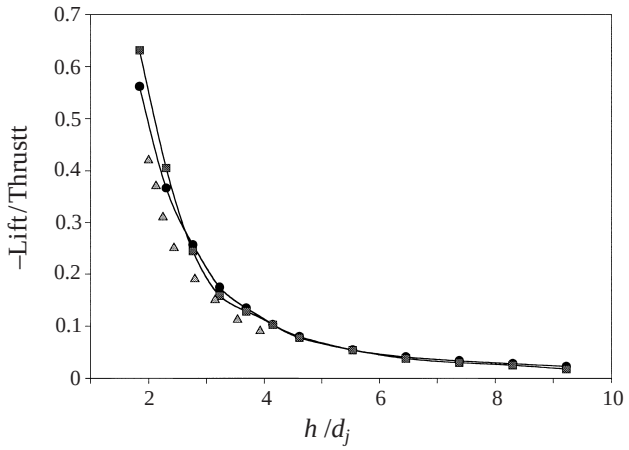

FIGURE 14. Lift loss variation with ground plane distance. ●, Mach 1.5, NPR=3.7; ■, Mach 1.0, NPR=3.7; ▲, Levin & Wardwell (1997), NPR=2.75.

Further downstream, the flow gradually decelerates, presumably through a system of compression waves, until it reaches sonic velocity. An examination of figure 13(*a*) reveals that the sonic condition occurs at $x = 86$ mm ($x/d \sim 3.4$) which corresponds to a change in axial velocity gradient. In contrast, the centreline mean velocity profile of the underexpanded jet (NPR = 5), shown in figure 13(*b*), displays a more drastic deceleration downstream of $x \sim 84$ mm ($x/d \sim 3.3$), indicating the presence of a much stronger shock than the ideally expanded case. Indeed, as pointed out earlier, the flow visualization clearly indicates the presence of this normal shock, commonly referred to as stand-off shock. Ideally, the velocity gradient across a normal shock will be extremely high. However, owing to particle lag inherent in PIV measurement, the velocity gradient across strong shock will be somewhat smeared, as evident in figure 13(*b*).

From the examination of all the instantaneous velocity fields, it is observed that critical changes in the jet flow field primarily occur in the vicinity of the jet impingement region (figure 6). This region extends as much as one jet diameter upstream of the ground plane. The behaviour of the flow field in this region is essential for understanding the ground erosion problem, a topic that is outside the scope of this paper but is the subject of an ongoing study (Alvi & Iyer 1999).

3.3. *Hover lift loss*

The negative jet-induced lift force that acts on the lift plate in the vicinity of the ground plane was obtained from the measurements of mean surface pressure. The estimation of the magnitude of this force becomes important as the ground plane approaches the nozzle exit. Typical variation of the negative lift force with h/d_j (d_j is the fully expanded jet diameter) is shown in figure 14. The lift force is normalized with the jet thrust calculated using one-dimensional isentropic equations. Included in the plot are the data of an underexpanded jet issuing from a conical nozzle. As the ground planes approach the lift plate, a large downward force is generated. For example, at $x/d = 2$, the magnitude of the lift loss is about 60% of the primary jet thrust. This force decreases rapidly in magnitude with increasing h/d and approaches an asymptotic value of the free jet, as shown in the figure. A comparison of the lift loss behaviour between the ideally expanded and underexpanded jet indicates that

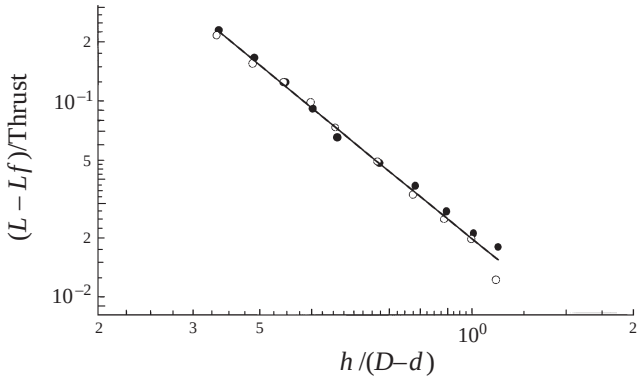

FIGURE 15. Lift loss correlation at NPR = 3.7. •, Mach 1.5 nozzle; ○, Mach 1.0 nozzle; ——, $0.02\ x^{-2.24}$.

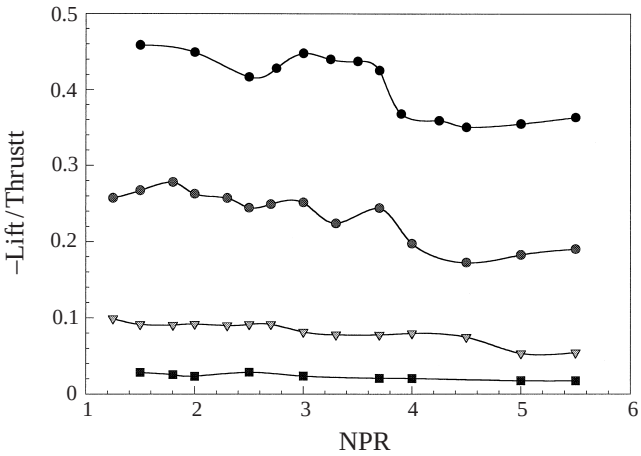

FIGURE 16. Lift loss variation with NPR for a sonic nozzle. ●, $h/d = 2.5$; ⊕, 3; ▽, 5; ■, 10.

the shock cells appear to play an insignificant role, except when the ground plane is in close proximity to the jet exit. This issue will be further explored later. Also included in the figure is the data for an underexpanded jet (NPR = 2.75) taken from Levin & Wardwell (1997). Their measurements were obtained directly using a thrust balance and a sonic nozzle. The agreement between the two sets of data provides confidence in the present data which were obtained from integrated surface pressure profiles on the lift plate.

Figure 15 shows the same data plotted in coordinates that are commonly used in the literature related to this subject. The data shows a linear variation which can be described by the following simple relation:

$$(L - L_f)/T = 0.02\ (h/(D-d))^{-2.24}.$$

Here, L is the downward force on the plate; L_f is the downward force on the plate for a free jet; T is the jet thrust, D is the diameter of the lift plate and d is the nozzle throat diameter. This relationship is very similar to that obtained by Levin & Wardwell (1997).

The dependence of lift loss on NPR was further explored to investigate the role of

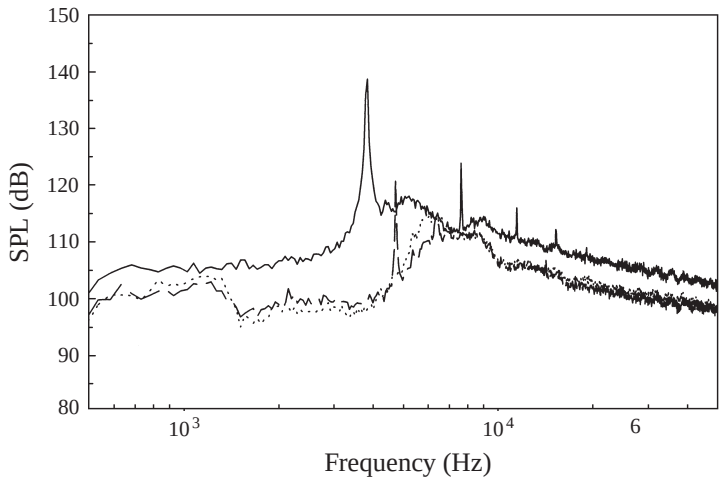

FIGURE 17. Near-field narrowband frequency spectra for $M = 1.5$ nozzle with and without the lift plate. ..., NPR=3.7, free jet, no lift plate; — -, 3.7, free jet, with lift plate; —, 5.0, free jet, with lift plate.

the shock cell structure at small values of h/d. A summary of these measurements for the sonic nozzle is provided in figure 16. This plot confirms the earlier assertion that the shock cells are only relevant for small h/d. Measurable variations in lift loss with NPR are only observed for $h/d \leqslant 3$. As alluded to in § 1 this nonlinear loss in lift was also observed by previous investigators (Levin & Wardwell 1997). It is speculated that the NPR range over which these variations are observed are, in part, related to the appearance of the stand-off shock and associated bubble. For small h/d, the scale and the unsteady characteristics of this stand-off shock are likely to influence the local entrainment velocities, thereby affecting the surface pressure and the resulting lift loss. Furthermore, at such small lift-to-ground plane separations, the entrainment properties of the high-speed (transonic to supersonic) wall jet are likely to play an important role in determining the local pressure field and lift loss.

3.4. *Acoustic characteristics*

3.4.1. *Screech tone characteristics*

It is well known that the noise from a supersonic jet existing from a C–D nozzle, operating away from the design condition, exhibits discrete tones commonly known as screech tones. The characteristics of these tones have been the subject of intense investigations; a summary of these studies can be found in review articles by Tam (1991, 1995). The mechanism for screech-tone generation is a feedback loop that is well understood. The presence of sound-reflecting surfaces in the immediate neighbourhood of the jet will alter the screech characteristics (Poldervaart, Wijnands & Bronkhorst 1973). In addition, a thick nozzle lip increases the screech intensity by about 10 dB (Norum 1983). Hence, the lift plate at the nozzle exit is expected to influence the screech tones. The near-field noise spectrum was measured for the free jet, with and without the lift plate, to examine its influence on the screech frequency and amplitude.

Figure 17 shows a typical narrowband spectrum of a near-field microphone signal, for a free jet at NPR = 3.7 (nominally ideally expanded). As expected, the spectrum shows no discernible discrete tones corresponding to screech. A broad peak corre-

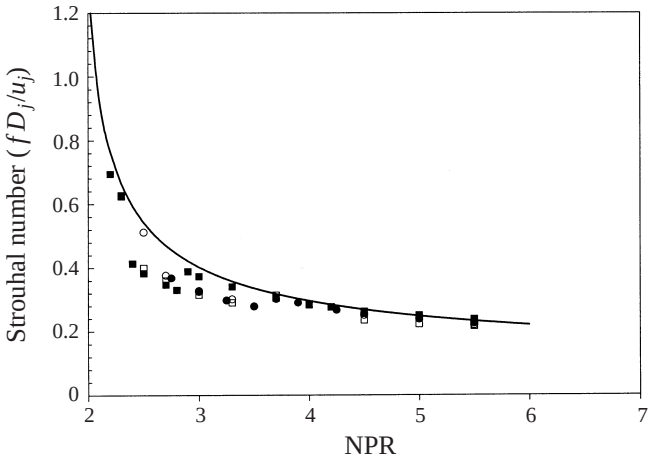

FIGURE 18. Free-jet screech tone variation with NPR. ○, Mach 1.5 nozzle, no lift plate; ●, Mach 1.5 nozzle, with lift plate; □, Mach 1 nozzle, no lift plate; ■, Mach 1 nozzle, with lift plate; –, Tam's prediction.

sponding to the broadband shock-associated noise (generated because of the presence of the weak shock cell structure) is present at this condition. However, in the presence of the lift plate, a distinct tone appears in the spectrum, as shown in the figure. Consistent with previous observations, the presence of the lift plate increased the amplitude of the screech tone. When the jet is underexpanded, the tones will become much stronger, resulting in several harmonics, as shown in the figure for NPR = 5.0. The tones measured in the present study are compared with the prediction formula given by Tam (1991), which has been thoroughly validated against a number of earlier measurements. Figure 18 shows a comparison of the data with Tam's prediction. Tam's formula only accounts for the helical mode, hence, in jets where symmetric or toroidal modes are present, primarily at NPR below 3, the data deviate from the curve. The good agreement of the data with the theoretical prediction for higher NPRs suggests that, although its magnitude is enhanced, the screech Strouhal number is not measurably altered by the presence of the lift plate. The effect of impingement on the screech frequency will be discussed in the following section.

3.4.2. *Impinging tones*

In addition to the screech tone, another dominant discrete tone appears when the jet impinges on the ground plate. These tones are commonly referred to as impinging tones (Krothapalli 1985; Powell 1988). Several different prediction formulae exist in the literature for the frequency prediction of these tones. Using the present experimental data, and in light of the measurements of the convection velocity of the large-scale vortices in the shear layer of the jet, the feedback loop will be further examined in this section.

Typical near-field narrowband spectra of an impinging jet at NPR = 3.7 for three different h/d are shown in figure 19. For the sake of clarity, the $h/d = 4$ and 4.25 spectra are displaced relative to the $h/d = 3.75$ spectra as follows: $h/d = 4$ by 10 dB and $h/d = 4.25$ by 20 dB. The shock cell structures are very weak at this NPR, as indicated by the PIV measurements. The spectra show the presence of several distinct tones, and a slight change in h/d can result in a significant change in the magnitude and frequency of these tones. In order to identify the origins of these tones,

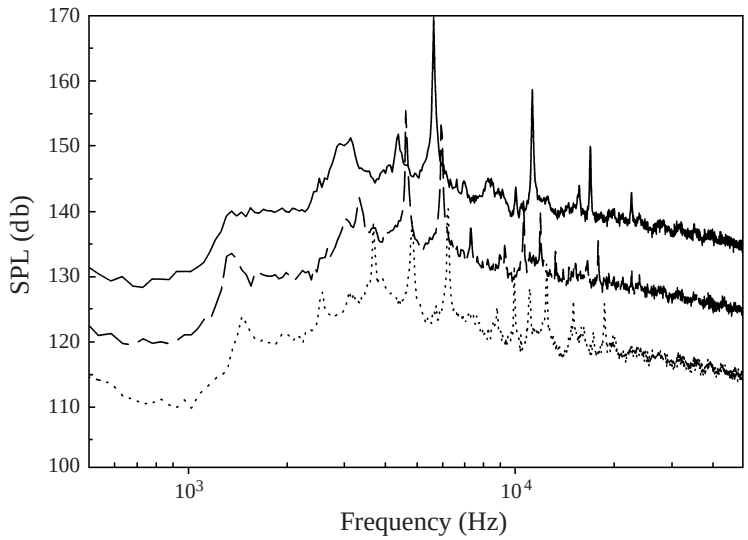

FIGURE 19. Near-field narrowband spectra for $M = 1.5$ impinging jet. …, NPR = 3.7, $h/d = 3.75$; — -, NPR = 3.7, $h/d = 4$; NPR = 3.7, $h/d = 4.25$.

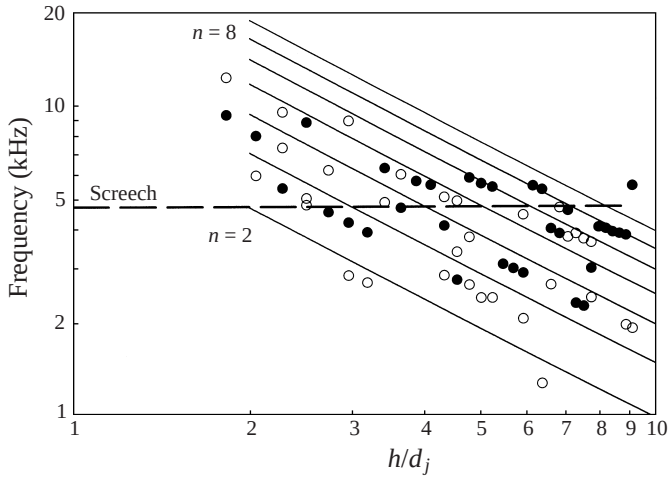

FIGURE 20. Impinging tone variation with ground plane distance for an ideally expanded jet, NPR = 3.7, $M_d = 1.5$. Comparison with —, the feedback formula assuming phase lag, $p = 0$. •, amplitude dominant tones.

a summary plot of their variation as a function of h/d is shown in figure 20 where the solid symbols represent the amplitude-dominant tones. The data fall roughly along parallel lines, in accordance with the well-known staging behaviour. Such a variation of frequency with the impinging plate height suggests that a feedback mechanism is governing the flow. Also shown in the figure, is the free-jet screech frequency, indicated by the dotted line. From the data, it appears that, in most cases, the dominant tones do not lie on the free-jet screech line. This suggests that the majority of the tones are generated because of jet impingement.

In order to predict the frequency variation with h/d shown in figure 20, the feedback-loop formula (equation (1)) was used. The convection velocities used in the

formula are obtained from the PIV measurements and a phase lag of zero, i.e. $p = 0$ was assumed. The solid lines shown in figure 20 represent the predicted frequencies using the feedback formula. They clearly do not agree with the measured tones. This is in contrast to the observations made for subsonic jets where, assuming a zero phase lag, the feedback formula predicts the tones reasonably well. To account for this discrepancy in the measured and predicted frequencies, one must re-examine the use of the feedback formula and ask whether any significant physical mechanisms responsible for generating impinging tones have been neglected. One such candidate was suggested by Henderson & Powell (1993) for underexpanded jets where they propose that oscillations of the stand-off shock play an important role in the generation of tones. Accordingly, Henderson & Powell (1993) proposed a modified feedback formula which accounts for stand-off shock oscillations. However, in the present case, the flow-visualization pictures and the PIV data indicate that the sound emanates from the jet impingement region and there is no appearance of a stand-off shock. This is because only weak shock cells are present in the jet, and the flow approaching the plate transitions through a series of compression waves, as indicated by the smooth variation of the centreline velocity in the impingement region (figure 13*a*). Hence, it is suggested that the feedback model of Powell (1988) which includes stand-off shock oscillations as a dominant source of sound may not be valid here. Consequently, a different source for this discrepancy had to be accounted for in the feedback mechanism.

The mechanism by which instability waves are produced by the incident sound wave at the nozzle exit is assumed to be quite simple in arriving at the feedback formula given earlier. A strong coupling between the sound wave and the instability waves takes place over the distance of a few instability wavelengths immediately downstream of the nozzle exit. A comprehensive discussion of this aspect can be found in Tam (1978) and Ahuja & Tam (1982). In the present case, the presence of the lift plate generates reflected waves (figure 4). These reflected waves, along with the upstream propagating waves, are expected to interact with the shear layer near the nozzle exit to generate instability waves. Consequently, this interaction between these acoustic waves and the shear layer near the nozzle exit may be much more complex and requires further investigation. As mentioned earlier, Powell argued that the phases of the acoustic wave and of the convected large-scale disturbances do not necessarily exactly correspond to each other at the nozzle exit and the source. This may be accentuated in this particular case by the reflective surface at the nozzle exit. It is suggested that the complex interaction between the instability waves and the acoustic waves will lead to a phase lag. Therefore the assumption of a zero phase lag, $p = 0$, is probably incorrect and the likely source of discrepancy between predicted and measured frequencies in figure 20. Good agreement with the prediction formula is obtained when the phase delay is accounted for using $p = -0.4$. The agreement can be clearly seen in figure 21 in which data from figure 20 is replotted using this value of p.

To examine the effect of shock cells on the tones, a limited number of data for an underexpanded jet at NPR = 5 ($M = 1.5$ nozzle) were also obtained. Similar to behaviour observed for the ideally expanded case (NPR = 3.7), there is a significant discrepancy between the predicted and measured impingement tones when a zero phase lag is assumed. As before, assuming the same value of $p = -0.4$ resulted in good agreement between the predicted and measured frequencies. This suggests that either the stand-off shock oscillations play a minor role or their effect is accounted for in the phase lag, p. Another reason for this difference may be due to the under-

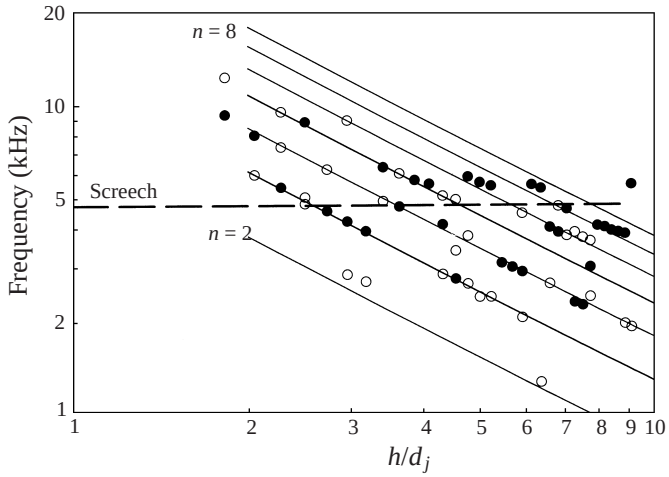

FIGURE 21. Impinging tone variation with ground plane distance for an ideally expanded jet, NPR = 3.7, $M_d = 1.5$ (same as figure 20). Comparison with —, the feedback formula assuming phase lag, $p = -0.4$. •, measured tones.

prediction of the convection velocities of the large-scale structures, as pointed out in the discussion of figure 9 (§ 3.2). Note that the particular value of the phase lag used here was not obtained from a rigorous analysis, rather this value of p simply provided the best agreement with the predicted frequencies over a wide range of conditions. Unfortunately, the relative contributions of the stand-off shock oscillation, under-prediction of convective velocities and the actual phase lag, to the total value of p used here cannot be determined. It should also be noted that for highly underexpanded jets, the stand-off shock oscillations are likely to play more significant role in determining the feedback loop.

Because of the confined nature of the geometry formed by the lift plate and the ground plane, some of the oscillatory modes can be strengthened. In cases where the screech or the impinging tone frequency matches the 'duct' mode, standing waves can be produced (Krothapalli & Hsia 1996). Such waves can be seen clearly in figure 4(*b*). Messersmith (1995) also made similar observations.

3.4.3. *Overall noise*

From the near-field narrowband spectra, overall sound pressure levels were calculated and plotted as a function of NPR in figure 22. A comparison of the $M = 1.5$ free jet, with and without the lift plate, shows that the plate has negligible influence on OASPL. However, in the presence of the ground plate, a significant increase in the OASPL was observed. For example, at the nearly ideally expanded condition at NPR = 3.7, an increase of about 8 dB is observed. The magnitude of the increase in OASPL owing to the impingement is consistent with the full-scale measurements obtained by Soderman (1990). A comparison of $h/d = 3$ and 5 shows that the location of the ground plate height for small h/d does not produce significant variations in OASPL.

4. Conclusions

The understanding of the oscillatory nature of impinging supersonic jets and their associated noise is of paramount importance for predicting the mean and

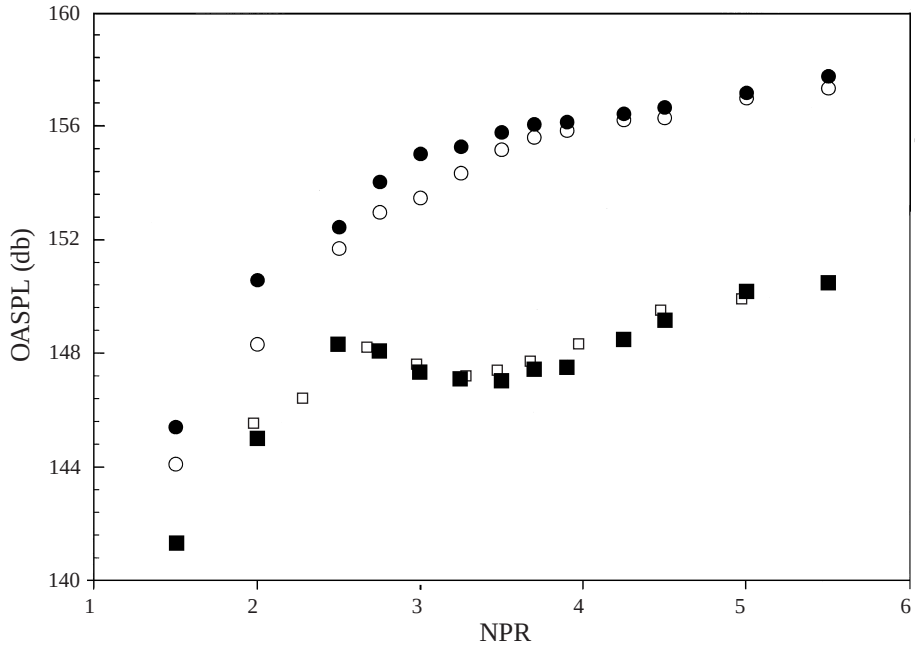

FIGURE 22. Near-field over all sound pressure level variation with NPR for $M = 1.5$ nozzle. ●, $h/d = 3$; ○, $h/d = 5$; □, free jet, no plate; ■, free jet, with plate.

unsteady loads on the airframe from which the jets are issuing. The experimental results described in this paper include lift loss, whole field velocity and acoustic measurements. Considered as a whole, these complementary measurements provide a coherent picture of the flow field associated with the oscillatory impinging supersonic jets and their near-field acoustic characteristics.

The self-sustained oscillatory behaviour of the impinging supersonic jet generates large-scale coherent vortical structures in the flow. These structures play a primary role in determining the entrainment properties of the jet and the acoustic field. From a practical perspective, knowledge of the entrainment flow is essential towards an understanding of the lift loss mechanism. Similarly, an understanding of the acoustic properties is important for predicting the unsteady acoustic loads on the airframe. A unique contribution of this study is the use of a novel high-resolution PIV technique to obtain the velocity field information with a high degree of accuracy. The velocity data clearly show that, as the ground plane approaches the nozzle exit, large-scale vortical structures of the increasing strength are generated. As a result, the jet entrainment velocities in the vicinity of the lift plate are significantly increased. This leads to lower pressures on the lift plate, followed by a suckdown force or lift loss. In the present study, suckdown forces as high as 60% of the primary jet thrust were measured. A significant reduction in thrust loss can be accomplished by eliminating the self-sustained oscillations of the jet. For example, the impinging tone could be suppressed and stopped by placing a small plate normal to the centreline of the jet in the outside ambient flow region (Karamcheti *et al.* 1969; Elavarasan, Venkatakrishnan & Krothapalli 1998).

The self-sustaining oscillation frequencies of the jet are frequently predicted using a feedback mechanism. Models describing this mechanism require a knowledge of the convection velocity of large-scale vortices in the shear layer. Using the vorticity

as a tracer quantity, the convection velocities of the large structures in the impinging jets were accurately measured. It was found that when the jet is operating in close proximity to the ground plane, the convection velocity of the structures is smaller than that of free jets ($0.52\,U_j$; U_j is the jet exit velocity). Using the measured convection velocities in a feedback formula, an accurate prediction of the measured frequencies was obtained. However, the amplitude determination remains elusive.

Near-field acoustic measurements indicate that the presence of the ground plane increases the OASPL by approximately 8 dB over a corresponding free jet. This increase was relatively insensitive to variations in the nozzle pressure ratio (NPR) for $\mathrm{NPR} > 3$.

This study briefly addressed the role of shock cells on the features discussed above. The convection velocities of the vortical structures was found to increase in the presence of shock cells. Except for very close ground plane proximity, the shock cells have a negligible influence on the suckdown force. For moderately underexpanded jets, the feedback mechanism appeared to be unaffected by the shock cells. When the jets are operating at highly underexpanded conditions, a strong highly unsteady shock cell structure is present. A detailed study is currently underway to examine its effects on the features discussed in this paper.

We would like to thank the continued support of NASA Ames Research Centre through a grant monitored by Mr Douglas Wardwell. Dr R. Elavarason and Dr L. Venkatakrishnan, helped us immensely in acquiring and processing the PIV data.

REFERENCES

Ahuja, K. K. & Tam, C. K. W. 1982 A Note on the coupling between flow instabilities and incident sound. *J. Sound Vib.* **83**, 433–439.

Alvi, F. S. & Iyer, K. G. 1999 Mean and unsteady flowfield properties of supersonic lmpinging jets with lift plates. *AIAA Paper* 99-1829.

Donaldson, C. DuP. & Snedeker, R. S. 1971 A study of free jet impingement. Part 1. Mean properties of free and impinging jets. *J. Fluid Mech.* **45**, 281–319.

Elavarasan, R., Venkatakrishnan, L., Krothapalli, A. & Lourenco, L. 1998 A PIV study of a supersonic impinging jet. *Proc. Intl Conf. On Optical Technology and Image Processing in Fluid, Thermal and Combustion Flow, Yokohama, Japan, December 1998.*

Glaznev, V. N. 1977 Sound field of an underexpanded supersonic jet impinging on a barrier. *Sov. Phys. Acoust.* **23**, 142–145.

Henderson, B. & Powell, A. 1993 Experiments concerning tones produced by an axisymmetric choked jet impinging on flat plates. *J. Sound Vib.* **168**, 307–326.

Ho, C. M. & Nosseir, N. S. 1981 Dynamics of an impinging jet. Part 1. The feedback phenomenon. *J. Fluid Mech.* **105**, 119–142.

How, S. & Tam, C. K. W. 1998 Numerical simulation of generation of axisymmetric mode jet screech tones. *AIAA Paper* 98-0283.

Karamcheti, K., Bauer A. B., Shields, W. L., Stegen, G. R. & Woolley, J. P. 1969 Some features of an edge tone flow field. *NASA SP* **207**, 275–304.

Krothapalli, A. 1985 Discrete tones generated by an impinging underexpanded rectangular jet. *AIAA J.* **23**, 1910–1915.

Krothapalli, A. & Hsia, Y. C. 1996 Discrete tones generated by a supersonic jet ejector. *J. Acoust. Soc. Am.* **99**, 777–784.

Krothapalli, A., Soderman, P. T., Allen, C. S., Hayes, J. A. & Jaeger, S. M. 1997 Flight effects on the far-field noise of a heated supersonic jet. *AIAA J.* **35**, 952–957.

Kuhn, R. E. 1977 Pressures and forces induced by the ground vortex. *Proc. Intl Powered Lift Conf. SAE P-306, March 1997*, pp. 35–44.

Kuo, C. Y. & Dowling, A. P. 1996 Oscillations of a moderately underexpanded choked jet impinging upon a flat plate. *J. Fluid Mech.* **315**, 267–291.

LAMONT, P. J. & HUNT, B. L. 1980 The impingement of underexpanded axisymmetric jets on perpendicular and inclined flat plates. *J. Fluid Mech.* **100**, 471–511.

LEVIN, D. B. & WARDWELL, D. A., 1997 Single jet-induced effects on small scale hover data in ground effect. *J. Aircraft* **34**, 400–407.

LOURENCO, L. M. & KROTHAPALLI, A. 1998 Mesh-free second order accurate algorithm for PIV processing. *Proc. Intl Conf. On Optical Technology and Image Processing in Fluid, Thermal and Combustion Flows, Yokohama, Japan, December 1998*, p. 224.

MARGASON, R., ARLEDGE, T. K., WARDWELL, D. A., HANGE, C. & NAUMOWICZ, T. 1997 Jet efflux characteristics and their influence of STOVL aircraft propulsion-induced effects. *Proc. Intl Powered Lift Conf. SAE P-306, March 1997*, pp. 3–10.

MARSH, A. H. 1961 Noise measurements around a subsonic air jet impinging on a plane rigid surface. *J. Acoust. Soc. Am.* **33**, 1065–1066.

MESSERSMITH, N. L. 1995 Aeroacoustics of supersonic and impinging jets. *AIAA Paper* 95-0509.

NEUWERTH, G. 1974 Acoustic feedback of subsonic and supersonic free jet which impinges on an obstacle. *NASA TT* F-15719.

NORUM, T. D. 1983 Screech suppression in supersonic jets. *AIAA J.* **21**, 235–240.

POLDERVAART, L. J., WIJNANDS, A. P. J. & BRONKHORST, L. 1973 Aerosonic games with the aid of control elements and externally generated pulses. *AGARD Conf. Proc.* 131, Noise Mechanisms, pp. 20.1–20.4.

POWELL, A. 1953*a* On edge tones and associated phenomena. *Acoustica* **3**, 233–243.

POWELL, A. 1953*b* On the mechanism of choked jet noise. *Proc. Phys. Soc. Lond.* B **66**, 1039–1057.

POWELL, A. 1988 The sound-producing oscillations of round underexpanded jets impinging on normal plates. *J. Acoust. Soc. Am.* **83**, 515–533.

ROSS, C., LOURENCO, L. & KROTHAPALLI, A. 1994 PIV measurements in a shock-containing supersonic flow. 32nd Aerospace Sciences Meeting, *AIAA Paper* 94-0047.

SODERMAN, P. T. 1990 The prediction of STOVL noise-current semi-empirical methods and comparisons with jet noise data. *NASA Tech. Mem.* 102833.

SUTHERLAND, L. C. & BROWN, D. 1972 Prediction method for near field noise environments of VTOL aircraft. *AFFDL-TR* 71-180, AD 900405.

TAM, C. K. W. 1978 Excitation of instability waves in a two-dimensional shear layer by sound. *J. Fluid Mech.* **89**, 357–371.

TAM, C. K. W. 1991 Jet noise generated by large-scale coherent motion. *Aeroacoustics of Flight Vehicles: Theory and Practice, NASA RP* 1258, vol. 1, pp. 311–390.

TAM, C. K. W. 1995 Supersonic jet noise. *Ann. Rev. Fluid Mech.* **27**, 17–43.

TAM, C. K. W. & AHUJA, K. K. 1990 Theoretical model of discrete tone generation by impinging jets. *J. Fluid Mech.* **214**, 67–87.

WARDWELL, D. A., HANGE, C., KUHN, R. E. & STEWART, V. R. 1993 Jet-induced ground effects on parametric flat-plate model in hover. *NASA Tech. Mem.* 104001.